Electronic Supplementary Material (ESI) for Inorganic Chemistry Frontiers.

Supplementary information

Supercapacitive properties of amorphous MoS_3 and crystalline MoS_2 nanosheets in organic electrolyte

Parthiban Pazhamalai[a, #], Karthikeyan Krishnamoorthy[b, #], Surjit Sahoo[a],

Vimal Kumar Mariappan[a], Sang -Jae Kim[a, c, *]

[a] Nanomaterials and system lab, Department of Mechatronics Engineering,

Jeju National University, Jeju 63243, Republic of Korea.

[b] Nanomaterials and system lab, Department of Mechatronics Engineering,

Jeju National University, Jeju 63243, Republic of Korea.

[c]Department of Advanced Convergence Science and Technology, Jeju National University,

Jeju 63243, Republic of Korea.

[#]These authors contributed equally.

*Corresponding author Email: kimsangj@jejunu.ac.kr

S1. Experimental section

S1.1 Materials

Ammonium molybdate tetra hydrate $(NH_4)_2Mo_7O_{24}\cdot 4H_2O$, ammonium sulfide $(NH_4)_2S$, and acetonitrile (AN), were purchased from Dae Jung Chemicals, South Korea. The electrolyte tetraethylammonium tetrafluoroborate ($TEABF_4$) was purchased from Alfa-Aesar chemicals, South Korea.

S1.2 Preparation of ammonium tetrathiomolybdate $(NH_4)_2MoS_4$ precursor

The ammonium tetrathiomolybdate powders were prepared by using ammonium molybdate tetra hydrate and ammonium sulfide as starting materials as reported elsewhere[1]. Briefly, 6.25 g of $(NH_4)_2Mo_7O_{24}\cdot 4H_2O$ was added to 25 mL of distilled water following the addition of 7.5 mL ammonia and vigorously stirred using a magnetic stirrer. After that, 57 mL of $(NH_4)_2S$ solution was added into the above solution and the mechanical stirring process is continued for 30 min. Then, the entire solution was transferred into a water bath maintained at 80 ºC for 2 h. After completion of this process, it was cooled to room temperature and allowed crystallization process for 24 h. The resulting $(NH_4)_2MoS_4$ crystal was filtered, washed with distilled water, ethanol for several times and dried at room temperature for 12 h.

S1.3 Preparation of amorphous MoS_3 and crystalline MoS_2

A facile one step thermal decomposition method was used to prepare amorphous MoS_3 and crystalline MoS_2 powders[1–3]. Briefly, the $(NH_4)_2MoS_4$ crystal was treated in presence of N_2 atmosphere at 200 and 600 ºC which results in the formation of MoS_3, and MoS_2, respectively.

S1.4 Instrumentation

A Rigaku X-ray diffractometer system with Cu Kα radiation (operated at 40 KeV and 40 mA) was employed to examine the phase purity and crystallinity of $(NH_4)_2MoS_4$, MoS_3, and

MoS_2 powders. The Raman spectrum of $(NH_4)_2MoS_4$, MoS_3, and MoS_2 powders were obtained using a LabRam HR Evolution Raman spectrometer (Horiba Jobin-Yvon, France). The Raman system used an Ar^+ ion laser operating at a power of 10 mW with an excitation wavelength of 514 nm; a 10 s data-point acquisition time was used to acquire the data. The surface morphology of the MoS_3 and MoS_2 powders were examined using a field emission-scanning electron microscopy (FE-SEM, JSM-6700F, JEOL Instruments) and high resolution transmission electron microscopy (HRTEM; Jem 2011, Jeol cop.) with CCD 4k x 4k camera (Ultra Scan 400SP, gatan cop.) The chemical state of elements present in the MoS_3, and MoS_2 powders was investigated using X-ray photoelectron spectroscopy (XPS) measurements using ESCA-2000, VG Microtech Ltd. A high-flux X-ray source at 1486.6 eV (aluminium anode) and 14 kV was used for X-ray generation, and a quartz crystal monochromator was used to focus and scan the X-ray beam on the sample surface. The N_2 adsorption-desorption isotherms of the $(NH_4)_2MoS_4$, MoS_3, and MoS_2 powders were measured at 77 K using a NOVA 2000 system (Quantachrome, USA) and the pore size distribution was calculated using Horvath-Kawazoe (HK) method.

S1.5 Electrochemical characterization

The working electrode was fabricated by grounding active material (MoS_3 or MoS_2), carbon black, and PVDF in the ratio (90:5:5) with appropriate amount of NMP (solvent) in an agate-mortar until a uniform slurry was obtained. Then, the slurry was spin coated on stainless substrates at a 200 rpm and dried at 80 ℃ for 12 h. The electroactive mass loading of the active material (MoS_3 or MoS_2) coated on to the stainless-current collector was measured as 0.5 mg, as calculated from the difference between the mass of the current collector before and after coating of the active material using Dual-range Semi-micro Balance (AUW-220D, SHIMADZU) with an approximation of five-decimal points. The SSC device was fabricated in coin-cell (CR2032)

configuration using active material (MoS_3 or MoS_2) coated stainless steel current collectors as electrodes separated by Celgard membrane and 0.5 M $TEABF_4$/AN as electrolyte. The fabricated SSC device was crimped using Electric Coin Cell Crimping and Disassembling Machine (MTI Korea). The handling of electrolyte and fabrication of coin cell were carried out inside a glove box with less than 1 ppm of moisture and oxygen. The electrochemical measurements such as cyclic voltammetry (CV) at different scan rates, electrochemical impedance spectroscopy (EIS) analysis (in the frequency range 0.01 Hz to 100 kHz, at amplitude of 10 mV) and galvanostatic charge–discharge (CD) measurements at different current ranges for the fabricated SSC device were performed using Autolab PGSTAT302N electrochemical workstation.

S1.6 Electrochemical analysis

Determination of specific capacity from CV profiles:

The specific capacity of the MoS_3 and/or MoS_2 SSC device is calculated from the CV analysis using the relation[4]:

$$C = [\int IdV / (s \times M)] \quad \text{..... (1)}$$

Here *"C"* is the specific gravimetric capacity (mAh g^{-1}), "I" is the current (A), "s" is the scan rate (mV s^{-1}), and "M" is the mass of the electrode (g).

Determination of specific capacity from CD profiles:

The specific capacity of the MoS_3 and/or MoS_2 SSC device was calculated from the CD profiles using the relation[4]:

$$C = (I \times T_d) / (M \times 3.6) \quad \text{……. (2)}$$

Here *"C"* is the specific gravimetric capacity (mAh g^{-1}), *"I"* is the discharge current, *"T_d"* is the time required for discharge, *"M"* is the mass loading of the electroactive material, and *"ΔV"* is the potential window.

Determination of Energy and power density:

The energy and power density of the MoS_3 and/or MoS_2SSC device are calculated in terms of using the relations given below[4,5]:

$$E= [I \int V(t)dt]/ [M \times 3.6] \quad \ldots\ldots\ldots\ldots\ldots\ldots (3)$$

$$P = E / T_d \quad \ldots\ldots\ldots\ldots\ldots\ldots (4)$$

Here *"E"* and *"P"* are the energy and power density of the device, *"ΔV"* is the potential window, and *"T_d"* is the discharge time.

Determination of specific capacitance from EIS analysis:

The specific capacitance of MoS_3 and/or MoS_2 SSC device with respect to applied frequency obtained from the EIS analysis using the relation[6]:

$$C = 1/ (2\pi f z'') \quad \ldots\ldots\ldots\ldots\ldots\ldots (5)$$

Here "C" is the specific capacitance of the device, and "f" is the applied frequency, and "z''" is the imaginary part of impedance.

Determination of maximal power density from EIS analysis:

The maximal power density of MoS_3 and/or MoS_2 SSC device was obtained from the EIS analysis using the relation[7]:

$$P = V^2/4ESR \quad \ldots\ldots\ldots\ldots\ldots\ldots (6)$$

Here "V" is the voltage window of the device, and "ESR" is the equivalent series resistance of the device.

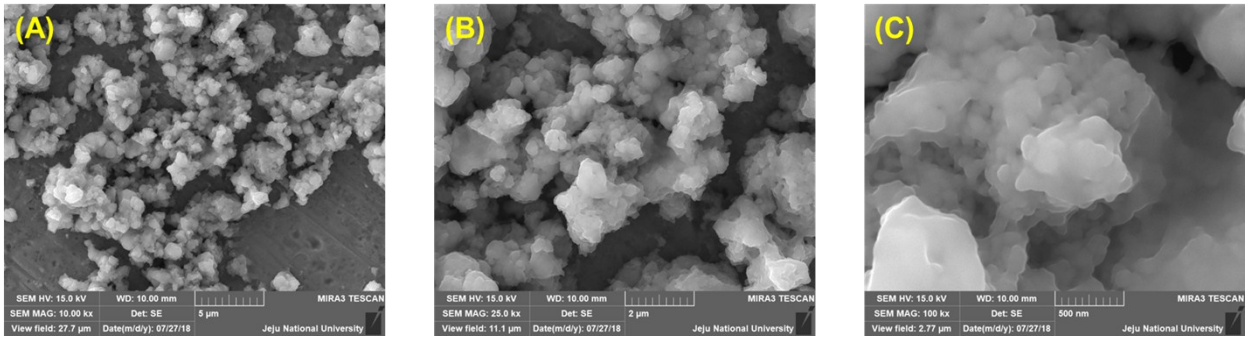

Figure S1. FE-SEM micrographs of MoS_3 obtained at different magnifications.

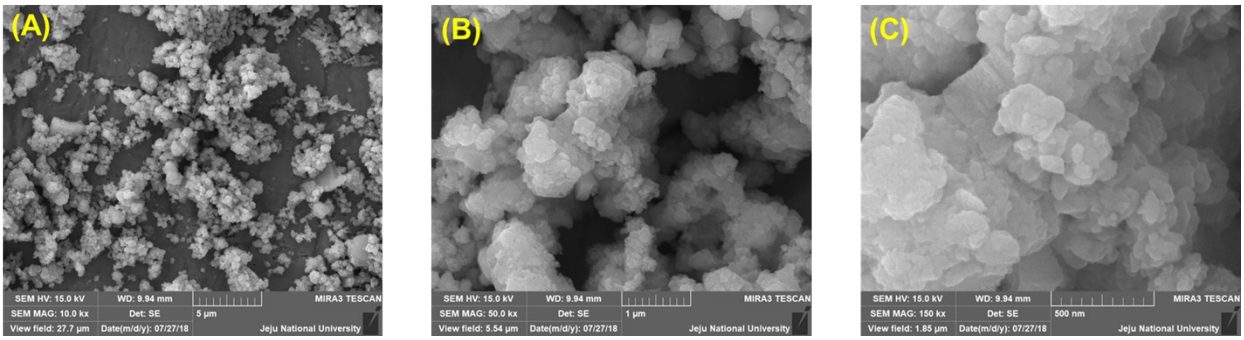

Figure S2. FE-SEM micrographs of MoS_2 obtained at different magnifications.

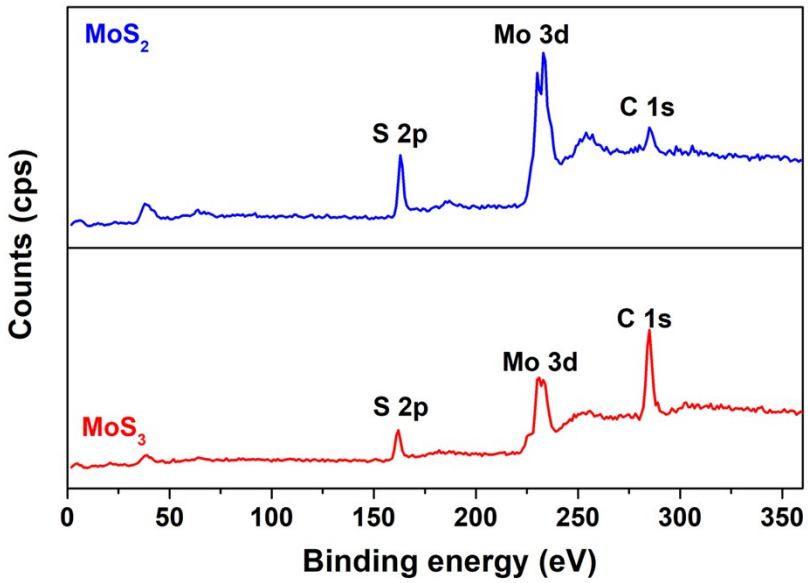

Figure S3. X-ray photoelectron survey spectrum of MoS_3 and MoS_2 sheets.

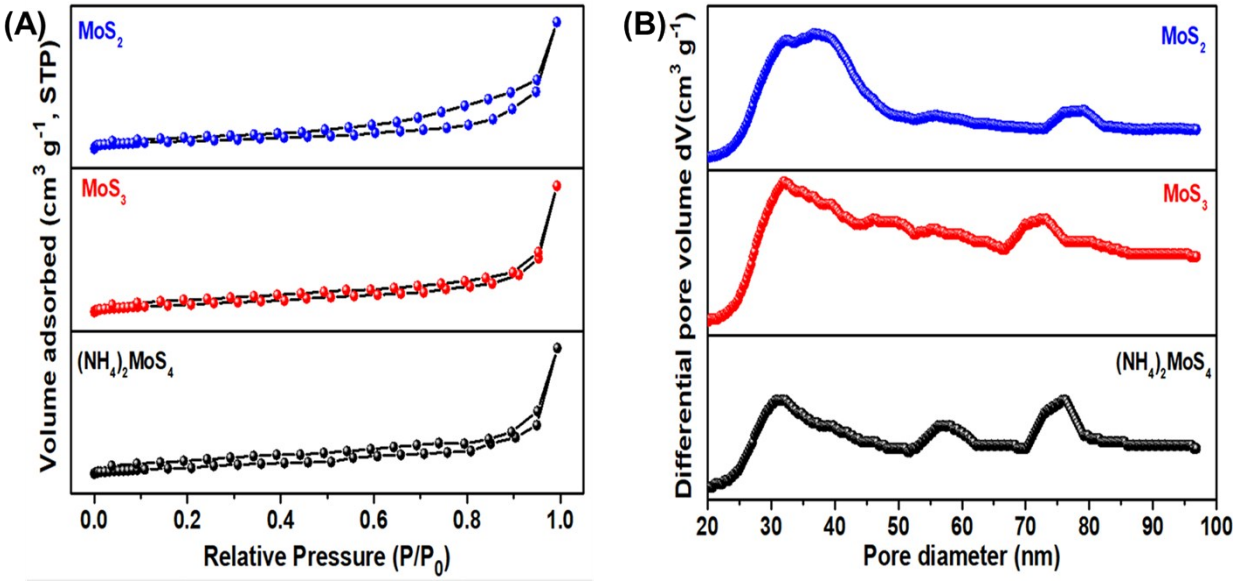

Figure S4. (A) N_2 adsorption–desorption isotherm and (B) pore size distribution of the $(NH_4)_2MoS_4$, MoS_3 and MoS_2.

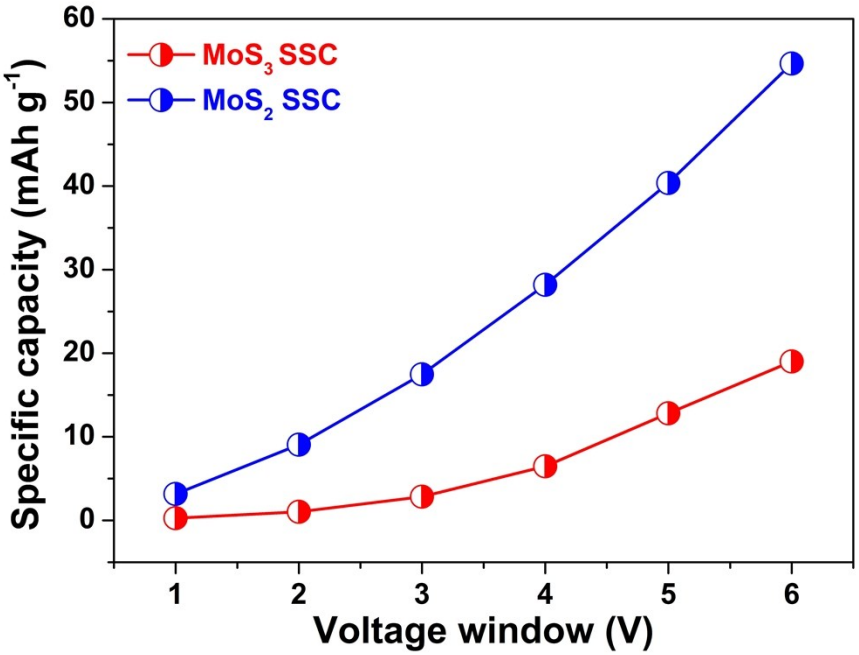

Figure S5. Effect of voltage window on the specific capacity of MoS_3 and MoS_2 SSC device measured in between the regime of -3 to +3 V.

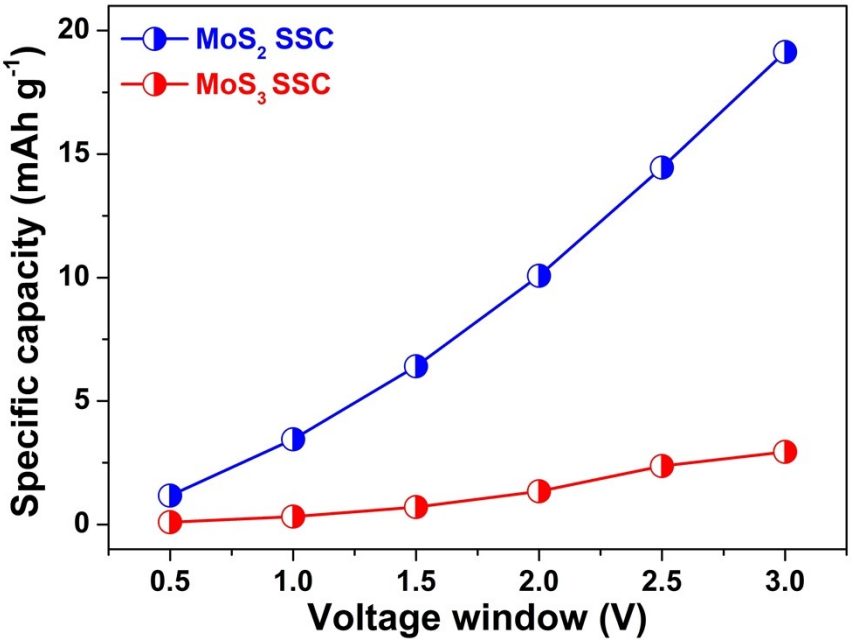

Figure S6. Effect of voltage window on the specific capacity of MoS_3 and MoS_2 SSC device measured in between the regime of 0 to +3 V.

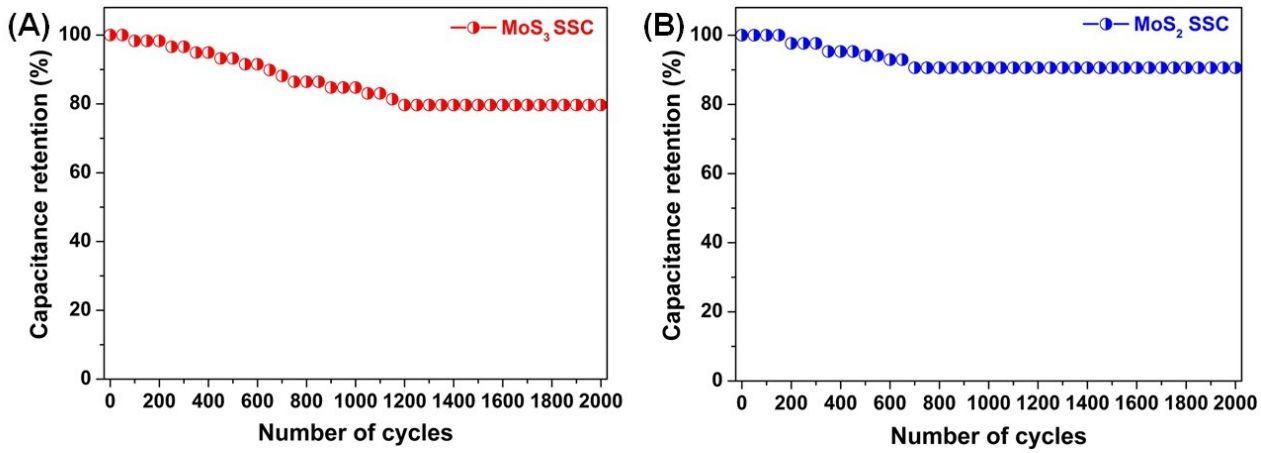

Figure S7. Cyclic stability analysis of MoS_3 and MoS_2 SSC device over 2000 cycles obtained using a current range of 1 and 2.5 mA, respectively. It shows that MoS_2 SSC devices higher capacitance retention of about 90 % of its initial capacitance whereas MoS_3 SSC device holds only 79.66 % of its initial capacitance after 2000 cycles.

Table S1: Comparitive performance metrics of MoS_2 and MoS_3 SSC with recently reported MoS_2 and other TMCs based SSCs

S.No.	Electrode material	Energy density (Wh kg^{-1})	Power density (W kg^{-1})	Reference
R1	RuS_2	1.51	40	[6]
R2	FeS	2.56	726	[8]
R3	MoS_2	5.42	128	[9]
R4	Ti_2CT_x Mxene	0.335	700	[10]
R5	Ti_2CT_x -500 Mxene	2.19	700	[11]
R6	RGO-CMK	23.1	250	[12]
R7	Monolithic biochar	20	2000	[13]
R8	CNT fiber	11.4	1000	[14]
R9	Graphene	18.9	1600	[15]
R10	Activated carbon	16	1100	[16]
R11	1T MoS_2	5	8550	[17]
R12	2H MoS_2	0.16	1500	[17]
R13	Commercial MoS_2	0.1	1500	[17]
R14	Mechanically exfoliated MoS_2 sheets	18.43	1125	[18]
R15	Siloxene	5.08	375	[19]
R16	MoS_3	3.39	323.29	This work
R17	MoS_2	20.68	496.71	This work

References:

1 T. Zhang, L.-B. Kong, Y.-H. Dai, K. Yan, M. Shi, M.-C. Liu, Y.-C. Luo and L. Kang, *Chem. - An Asian J.*, 2016, **11**, 2392–2398.

2 R. I. Walton, A. J. Dent and S. J. Hibble, *Chem. Mater.*, 1998, **10**, 3737–3745.

3 T. Wang, S. Chen, H. Pang, H. Xue and Y. Yu, *Adv. Sci.*, 2017, **4**, 1600289.

4 A. Laheäär, P. Przygocki, Q. Abbas and F. Béguin, *Electrochem. commun.*, 2015, **60**, 21–25.

5 K. Krishnamoorthy, P. Pazhamalai, G. K. Veerasubramani and S. J. Kim, *J. Power Sources*, 2016, **321**, 112–119.

6 K. Krishnamoorthy, P. Pazhamalai and S. J. Kim, *Electrochim. Acta*, 2017, **227**, 85–94.

7 D. Aradilla, P. Gentile, G. Bidan, V. Ruiz, P. Gómez-Romero, T. J. S. Schubert, H. Sahin, E. Frackowiak and S. Sadki, *Nano Energy*, 2014, **9**, 273–281.

8 S. S. Karade, P. Dwivedi, S. Majumder, B. Pandit and B. R. Sankapal, *Sustain. Energy Fuels*, 2017, **1**, 1366–1375.

9 M. S. Javed, S. Dai, M. Wang, D. Guo, L. Chen, X. Wang, C. Hu and Y. Xi, *J. Power Sources*, 2015, **285**, 63–69.

10 R. B. Rakhi, B. Ahmed, M. N. Hedhili, D. H. Anjum and H. N. Alshareef, *Chem. Mater.*, 2015, **27**, 5314–5323.

11 R. B. Rakhi, B. Ahmed, D. Anjum and H. N. Alshareef, *ACS Appl. Mater. Interfaces*, 2016, **8**, 18806–18814.

12 Z. Lei, Z. Liu, H. Wang, X. Sun, L. Lu and X. S. Zhao, *J. Mater. Chem. A*, 2013, **1**, 2313–2321.

13 J. Jiang, *J. Electrochem. Soc.*, 2017, **164**, H5043–H5048.

14 E. Senokos, V. Reguero, L. Cabana, J. Palma, R. Marcilla and J. J. Vilatela, *Adv. Mater. Technol.*, 2017, **2**, 1600290.

15 Y. Chen, X. Zhang, D. Zhang and Y. Ma, *Mater. Lett.*, 2012, **68**, 475–477.

16 A. Eftekhari, *Energy Storage Mater.*, 2017, **9**, 47–69.

17 S. Yang, K. Zhang, C. Wang, Y. Zhang, S. Chen, C. Wu, A. Vasileff, S.-Z. Qiao and L. Song, *J. Mater. Chem. A*, 2017, **5**, 23704–23711.

18 P. Pazhamalai, K. Krishnamoorthy, S. Manoharan and S. J. Kim, *J. Alloys Compd.*, 2019, **771**, 803–809.

19 K. Krishnamoorthy, P. Pazhamalai and S. J. Kim, *Energy Environ. Sci.*, 2018, **11**, 1595–1602.